THE JOURNAL OF PHYSICAL CHEMISTRY Letters

Letter

Cite This: J. Phys. Chem. Lett. 2018, 9, 1185−1194

pubs.acs.org/JPCL

Ultrafast, Self-Driven, and Air-Stable Photodetectors Based on Multilayer $PtSe_2$/Perovskite Heterojunctions

Zhi-Xiang Zhang,[†,∥] Long-Hui Zeng,[‡,∥] Xiao-Wei Tong,[†] Yang Gao,[†] Chao Xie,*[,†] Yuen Hong Tsang,[‡] Lin-Bao Luo,*[,†] and Yu-Cheng Wu*[,§]

[†]School of Electronic Science and Applied Physics and Anhui Provincial Key Laboratory of Advanced Functional Materials and Devices, Hefei University of Technology, Hefei 230009, PR China

[‡]Department of Applied Physics and Materials Research Center, Hong Kong Polytechnic University, Hung Hom, Kowloon, Hong Kong 99077, PR China

[§]School of Materials Science and Engineering, Hefei University of Technology, Hefei, Anhui 230009, PR China

Supporting Information

ABSTRACT: We report on the large-scale synthesis of polycrystalline multilayer $PtSe_2$ film with typical semimetallic characteristics. With the availability of the large-area film, we constructed a heterojunction composed of multilayer $PtSe_2$ and Cs-doped $FAPbI_3$, which can function as a self-driven photodetector in a broadband wavelength from the ultraviolet to the near-infrared region. Further photoresponse analysis revealed that the heterojunction device showed outstanding photosensitive characteristics with a large I_{light}/I_{dark} ratio of 5.7×10^3, high responsivity of 117.7 mA W^{-1}, and decent specific detectivity of 2.91×10^{12} Jones at zero bias. More importantly, the rise/fall times were estimated to be 78/60 ns, rendering our device the fastest device among perovskite-2D photodetectors reported to date. In addition, it was also observed that the $PtSe_2$/perovskite photodetector can almost retain its photoresponse properties after storage in ambient conditions for 3 weeks. This study suggests the potential of the present $PtSe_2$/perovskite heterojunction for future air-stable ultrafast photodetecting applications.

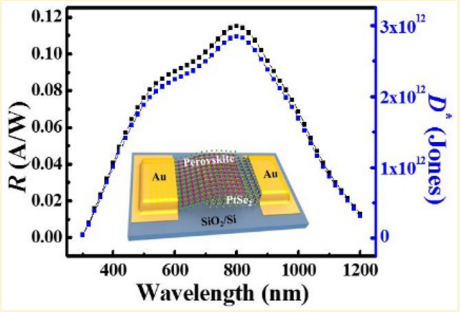

Hybrid organic−inorganic perovskites have recently emerged as a new class of revolutionary structures in a variety of optoelectronic applications including solar cells, light-emitting diodes, photodetectors, and lasers for their appealing optical and electrical properties (e.g., appropriate direct band gap, high optical absorption coefficient, low exciton binding energy, broadband light absorption, and so on).[1,2] Among these optoelectronic devices, particular attention has been devoted to developing high-performance photodetectors, which are of pivotal importance for both scientific and industrial purposes. To date, a number of photodetectors with different device configurations and working principles, including photoconductors, phototransistors, and photodiodes, have been extensively studied based on this group of materials.[3−6] From the perspective of high-frequency optical sensing applications, such as military warning, fast imaging, high-speed optical communication, and monitoring of ultrafast dynamic processes, photodetectors with ultrafast response speed and high sensitivity are highly desirable. Recent works have shown that perovskite photodiodes can exhibit inherent advantages in terms of faster response speed, lower noise, and larger specific detectivity over perovskite photoconductors/phototransistors.[3−6] These photodiodes usually have solar cell-like architectures and exploit perovskite as light-absorbing media to generate photocarriers and electron/hole transporting layers on opposite sides of the perovskite for photocarrier extraction.[7−10] For example, an intrinsic response speed as low as ∼1 ns has been demonstrated in a solution-processed perovskite photodiode, which represents the fastest perovskite photodetector to date.[10] However, the reported perovskite photodiodes normally have complex device structures and entail complicated multiple patterning steps for fabrication. Moreover, their air stability and durability are inevitably far from satisfactory because of the involvement of organic materials as transporting layers. In light of this, it is highly necessary to explore perovskite photodiodes that possess simpler device architectures, facile fabrication processes, and potentially higher air stability and durability.

As a rising material family, two-dimensional (2D) layered materials have proved to be ideal materials for building high-performance photodetectors as well.[11−14] For example, 2D layered materials have been successfully integrated with perovskites to assemble various hybrid phototransistors.[15−20] Benefiting from the synergistic effect, these devices showed improved responsivity and photoconductive gain, yet with spectral response range limited to ∼800 nm by the intrinsic light absorption of perovskite. For near-infrared (NIR) light

Received: January 26, 2018
Accepted: February 21, 2018
Published: February 21, 2018

DOI: 10.1021/acs.jpclett.8b00266
J. Phys. Chem. Lett. 2018, 9, 1185−1194

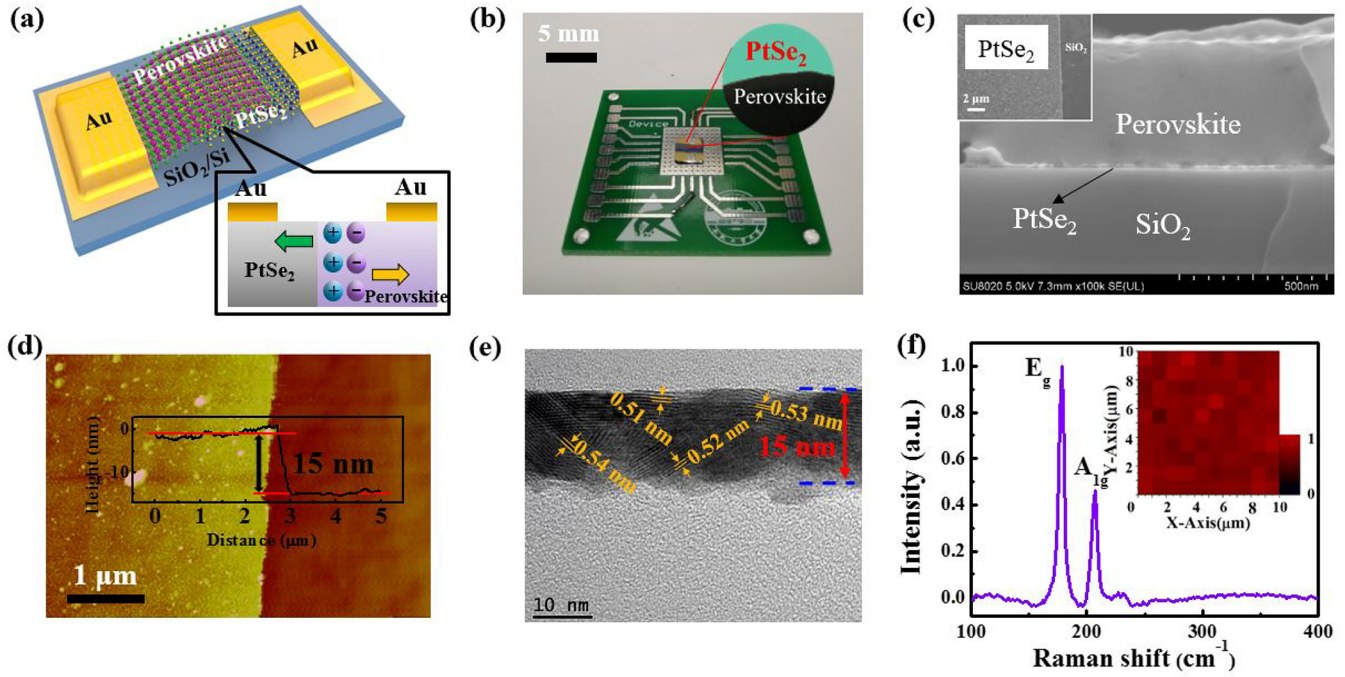

Figure 1. (a) Schematic illustration of the $PtSe_2$/perovskite heterojunction photodetector. The inset shows the built-in electric field at the $PtSe_2$/perovskite interface. (b) Digital photograph of the as-prepared device. (c) Cross-sectional SEM image of the $PtSe_2$/perovskite interface. The inset shows the FESEM image of the $PtSe_2$ film on the SiO_2/Si substrate. (d) AFM image of the $PtSe_2$ on SiO_2/Si substrate. The inset shows the height profile. (e) Cross-sectional FETEM image of the $PtSe_2$ film. (f) Raman spectrum of the as-prepared $PtSe_2$ thin film. The inset shows the 2D Raman mapping of the $PtSe_2$ film over an area of 10×10 μm^2.

detection, some researchers tried to hybridize perovskites with some narrow band gap materials, which act as NIR light absorbers,[21,22] or exploited photocarrier excitation from impurity energy levels within the band gap of perovskites.[23,24] Nevertheless, by virtue of long lifetimes of trapped carriers, the above perovskite phototransistors are often subject to very slow photoresponse (from millisecond to second), which greatly restricts their potential application in high-frequency optoelectronics. In addition, a 2D WSe_2/perovskite heterojunction with graphene electrodes has also been demonstrated recently, which exhibited distinct gate-tunable rectifying and photovoltaic effects.[25] However, the fabrication process relies strongly on mechanical exfoliation of the materials, making the device unsuited for large-scale production. The investigation of some crucial photoresponse characteristics, such as device noise, specific detectivity, spectrum response, etc., is also undemonstrated. Therefore, comprehensive study of photodiodes based on 2D layered material/perovskite heterojunctions is thus far lacking.

In this work, we developed a self-driven photodetector by combining perovskite with multilayer $PtSe_2$, a representative of the 2D layered materials that have recently found wide applications in various fields, including field-effect transistors, solar cells, photodiodes, and gas sensors, for its tunable band gap, high carrier mobility, and excellent air stability.[26−29] It is revealed that the as-assembled multilayer $PtSe_2$/perovskite heterojunctions were capable of operating over a wide spectrum region from the ultraviolet (UV) to the NIR (300−1200 nm). The heterojunction device exhibited outstanding optoelectronic characteristics in terms of large I_{light}/I_{dark} ratio of 5.7×10^3, high responsivity of 117.7 mAW^{-1}, respectable specific detectivity of 2.6×10^{12} Jones, and more importantly, ultrafast response speed of 78/60 ns, which renders our device the fastest perovskite-2D photodetectors to date. Additionally, the photoresponse characteristics can remain almost unchanged after the photodetector is stored in ambient condition for 3 weeks, showing robust air stability and long-term durability. The generality of the above findings suggests that the present heterojunction device holds huge possibility for future air-stable sensitive photodetectors with ultrafast response speed for practical applications.

Panels a and b of Figure 1 depict a schematic diagram and photograph of the $PtSe_2$/perovskite heterojunction photodiode, respectively. This special geometry is characterized by the formation of a built-in electric field at the interface, via which the device is capable of separating the electron−hole pairs in an efficient way. In this work, a large-scale $PtSe_2$ film was prepared via selenization of predeposited Pt layers, and Cs-doped $FACsPbI_3$ perovskite was employed as the light absorbing medium, which reportedly exhibits higher electron mobility and better air stability as compared to extensively used $MAPbI_3$ perovskite.[30−32] The detailed setup for synthesizing $PtSe_2$ film and the device fabrication procedure are shown in Figures S1 and S2, respectively. The field emission scanning electron microscopy (FESEM) analysis in Figure 1c shows the cross-sectional image of the $PtSe_2$/perovskite interface. Because of the difference in contrast, both $PtSe_2$ layer and perovskite film can be easily distinguished. Figure 1d displays the atomic force microscopy (AFM) image of the $PtSe_2$ film along with a height profile in the inset diagram, from which the thickness of the film is determined to be ∼15 nm, corresponding to ∼18 layers of single-layer $PtSe_2$.[26] Considering the thickness of the $PtSe_2$ is relatively high, it is reasonable to believe that the as-fabricated $PtSe_2$ is semimetal. A typical cross-sectional field emission transmission electron microscope (FETEM) image of $PtSe_2$ film is depicted in Figure 1e, revealing that the material is

DOI: 10.1021/acs.jpclett.8b00266
J. Phys. Chem. Lett. 2018, 9, 1185−1194

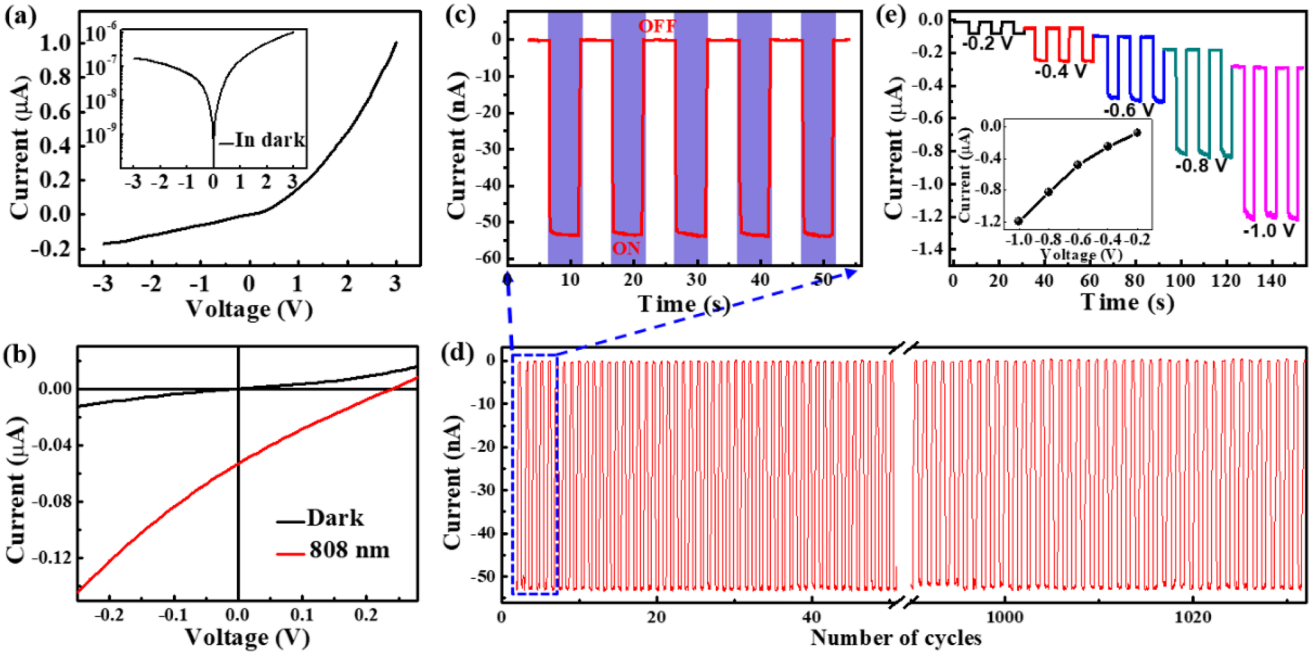

Figure 2. (a) $I-V$ characteristics of the $PtSe_2$/perovskite heterojunction in the dark at room temperature. The inset shows the curve in a semilogarithmic scale. (b) Comparison of $I-V$ characteristics of the $PtSe_2$/perovskite heterojunction photodetector in the dark and illuminated with 808 nm light (3.42 mW/cm^2). (c) Time-dependent photoresponse of the device under 808 nm light illumination (5.76 mW/cm^2) at zero bias. (d) Time-dependent photoresponse of the device over thousands of cycles of operation. (e) Time-dependent photoresponse of the device under 808 nm light illumination (7.96 mW/cm^2) at different bias voltages of −0.2, −0.4, −0.6, −0.8, and −1 V. The inset shows the photocurrent of the device as a function of the bias voltage.

polycrystalline with nanometer-sized crystalline domains of different thicknesses. The thickness derived from the image is coincident with the result from AFM measurement. In addition, the interlayer distance of the crystalline domains distributes from 0.48 to 0.59 nm, with an average value of 0.53 nm (Figure S4a), which is close to the value reported in the literature (0.52 nm).[33] Furthermore, th Raman spectrum in Figure 1f is composed of two distinct peaks located at 178 and 207 cm^{-1}, which can be assigned to the E_g in-plane vibrational mode of Se atoms and A_{1g} out-of-plane vibration mode, respectively.[34] In order to further investigate the uniformity of the $PtSe_2$ film, 2D Raman mapping over an area of 10 × 10 μm^2 was performed. The inset of Figure 1f reveals the intensity distribution of the representative peak at 178 cm^{-1} extracted from a set of Raman spectra. It is clear that the peak intensity displays a relatively narrow distribution, indicative of good uniformity of the as-synthesized $PtSe_2$ film with few defects. X-ray photoemission spectroscopy (XPS) analysis was conducted to study components and binding energies of the $PtSe_2$ film. As displayed in Figure S3, there are two peaks at 73.25 and 76.58 eV that are related to Pt $4f_{7/2}$ and Pt $4f_{5/2}$ orbitals, respectively, whereas the Se $3d_{5/2}$ and Se $3d_{3/2}$ orbitals of divalent selenium ions are observed at 54.58 and 55.65 eV, respectively. X-ray diffraction (XRD) pattern of the prepared $FA_{0.85}Cs_{0.15}PbI_3$ perovskite film was studied and is displayed in Figure S4b. The observed strong peaks can be well assigned to the diffraction peaks of black phase $FAPbI_3$ perovskite, indicating good crystallinity of the film. The surface morphology of the perovskite film was characterized by FESEM. As revealed in Figure S4c, it is apparent that high-quality continuous perovskite film with few pinholes and defects can be formed.

The as-fabricated device exhibited a nonlinear current−voltage ($I-V$) behavior (rectifying characteristic) in the dark with a rectification ratio of ∼10 at ±3 V (Figure 2a). Such a relatively low rectification ratio is likely due to the ion migration mediated by vacancies in perovskite that compensates the effective electric field applied on the heterojunction and thus prevents the current turning on at forward bias.[25] Given the good Ohmic contact of both Au-perovskite and Au-$PtSe_2$ (Figure S4e,f), the above nonlinear $I-V$ behavior arises solely from the heterojunction formed between $PtSe_2$ and perovskite. Figure 2b compares the $I-V$ curves of the device at different conditions. One can find with ease that once illuminated with 808 nm NIR light, the device displays a photovoltaic effect with an open-circuit voltage (V_{OC}) of 0.23 V and a short-circuit current (I_{SC}) of 53.1 nA under 3.42 mW/cm^2 illumination. Even though the power conversion efficiency is rather low (<1%), it however enables our device to operate as a self-driven photodetector working without a power supply. Figure 2c plots the time-dependent photoresponse of the heterojunction under alternative on/off NIR light at zero bias. Apparently, the device can be reversibly switched between low- and high-conductance states, giving rise to a stable and repeatable I_{light}/I_{dark} ratio of 3.8 × 10^3. The sharp rise and fall edges suggest that the photogenerated electrons and holes can be rapidly separated by the heterojunction and then collected by respective electrodes. In fact, such photoresponse is repeatable even after thousands of cycles of operation (Figure 2d), implying excellent reproducibility of our photodetector. It should be noted that time-dependent photocurrent is highly dependent on the operating bias voltage. The net photocurrent (I_{ph}) of the device can be extracted by deducing device current under light by dark current ($I_{ph} = I_{light} - I_{dark}$). As displayed in Figure 2e, the photocurrent increased monotonously with

DOI: 10.1021/acs.jpclett.8b00266
J. Phys. Chem. Lett. 2018, 9, 1185−1194

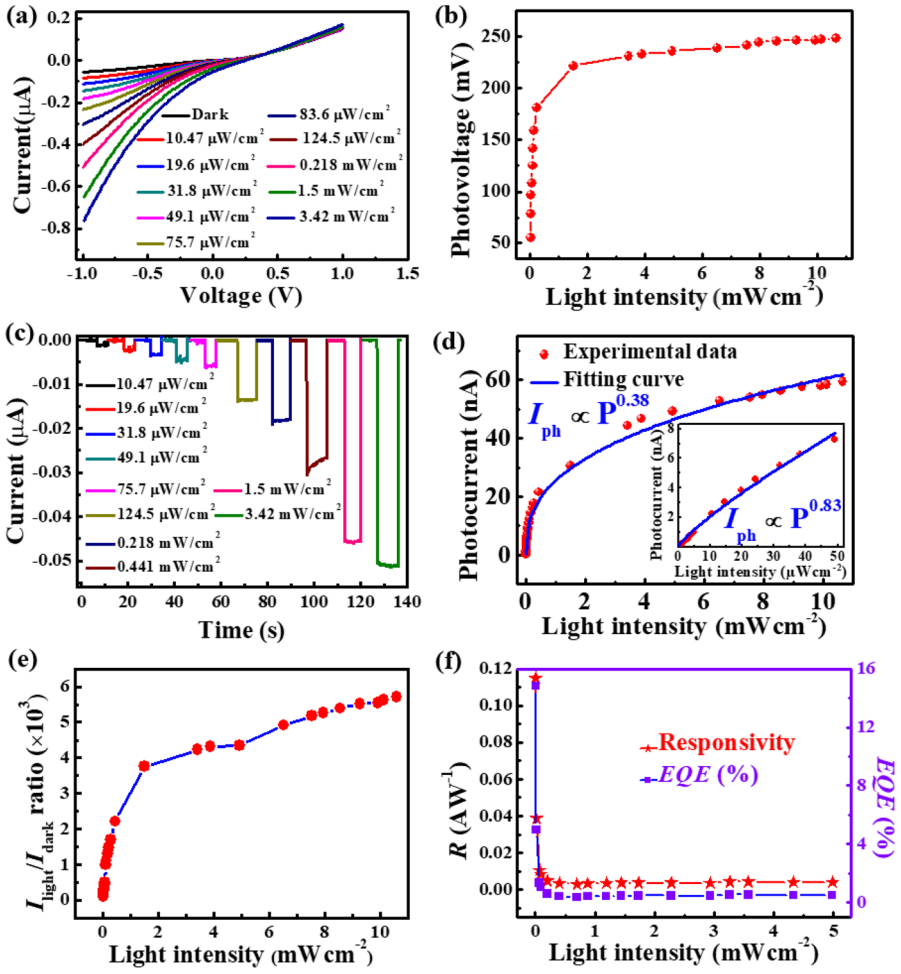

Figure 3. (a) $I-V$ curves of the $PtSe_2$/perovskite heterojunction photodetector under 808 nm light with different light intensities. (b) Photovoltage as a function of the incident light intensity. (c) Time-dependent photoresponse of the device under 808 nm light with various light intensities at zero bias. (d) Photocurrent as a function of incident light intensity at zero bias. The inset shows the dependence of photocurrent on light intensity in a narrow light intensity range. (e) Relationship between I_{light}/I_{dark} ratio of the device and light intensity at zero bias. (f) Responsivity and EQE of the device as a function of incident light intensity.

increasing reverse working bias, which is reasonable because a larger electric field toward the built-in one can significantly increase separation efficiency and drift velocity of photogenerated electrons and holes and therefore suppress their recombination activity.

The photoresponse characteristics of the heterojunction device are also strongly dependent on the incident light intensity. Figure 3a shows the $I-V$ curves of the device under NIR light of varied light intensities. It was observed that both photocurrent and photovoltage increased gradually with increasing light intensity, owing to the increased population of photogenerated charge carriers under higher light intensity. For example, the photovoltage increased rapidly from 55 to 181 mV when the light intensity changed from 10.47 to 218.2 μW cm^{-2}. Further increasing the light intensity, however, led to a slow increase in photovoltage (Figure 3b). Similar tendency was also found in the dependence of photocurrent on light intensity at zero bias (Figure 3c), and the photocurrent curve can be well fitted by a power law, $I_{ph} \propto P^{\theta}$, where θ is an exponent and determines the response of the photocurrent to light intensity. Fitting the curve in a wide light intensity range gave a θ = 0.38 (Figure 3d). This nonunity exponent value along with the above relationships of dependence of both photovoltage and photocurrent on light intensity is probably associated with the increased recombination activity of photogenerated charge carriers at elevated light intensity due to higher carrier density as well as the presence of some trap states between the Fermi level and the conduction band.[35] To verify the hypothesis, we then fitted the photocurrent curve in a low light intensity range (inset in Figure 3d), where a more ideal exponent θ = 0.83 was obtained, suggesting that recombination loss is relatively low in this light intensity region.[36] Therefore, we conclude that light intensity plays a critical role in determining carrier recombination activity and the photoresponse characteristics in our heterojunction photodetector. Besides photocurrent, the I_{light}/I_{dark} ratio of the photodetector was found to increase gradually with increasing light intensity, and the maximum value can be as high as 5.7 × 10^3 when the light intensity reaches 10.6 mW cm^{-2} (Figure 3e).

We then calculated responsivity (R) and external quantum efficiency (EQE), two crucial performance figure-of-merits, in order to quantitatively evaluate the device photoresponse performance. R is defined as the photocurrent generated per unit power of the incident light on the effective area of a photodetector, while EQE is the ratio between the number of electron−hole pairs with contribution to the photocurrent and the number of incident photons at a given wavelength, which are usually expressed by the following equation:[37]

DOI: 10.1021/acs.jpclett.8b00266
J. Phys. Chem. Lett. 2018, 9, 1185−1194

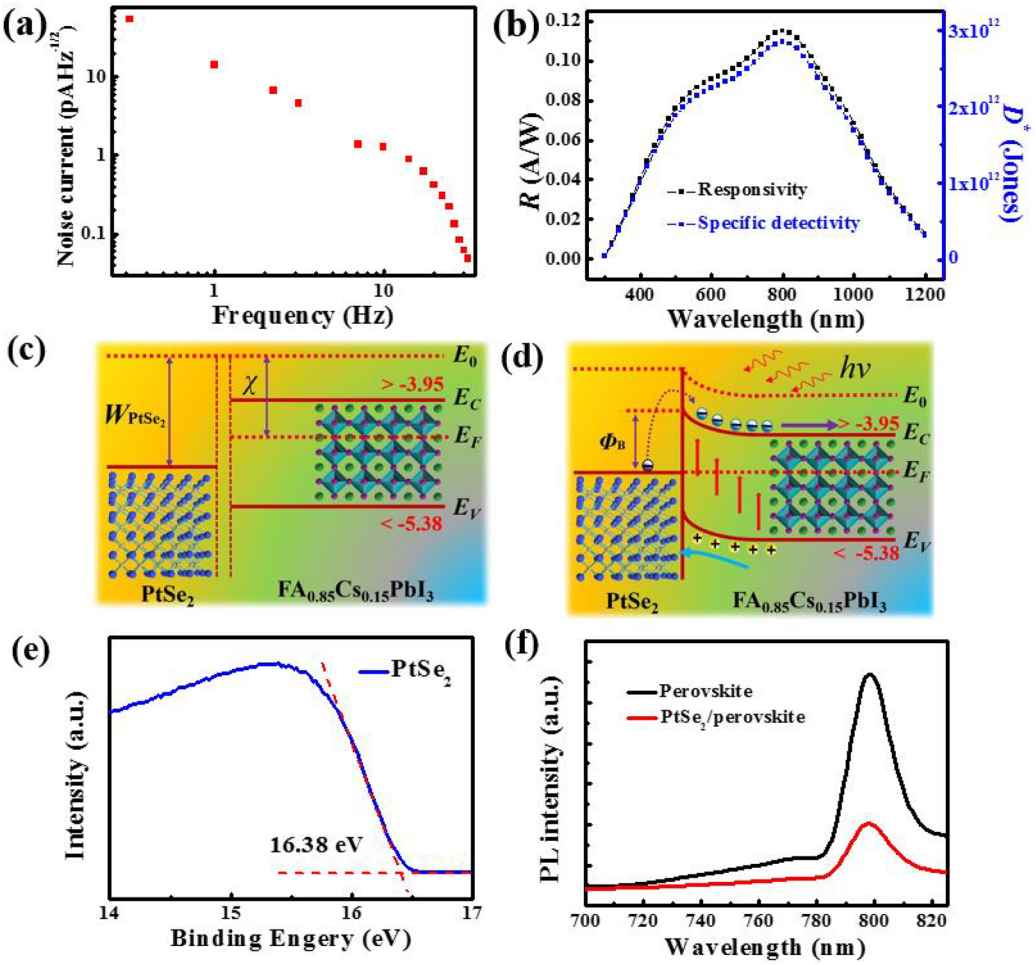

Figure 4. (a) Noise current of the device as a function of frequency. (b) Wavelength-dependent responsivity and specific detectivity of the device (from 300 to 1200 nm). (c) Energy band diagrams of the $PtSe_2$ and $FA_{0.85}Cs_{0.15}PbI_3$ perovskite. (d) Energy band diagram of the $PtSe_2$/$FA_{0.85}Cs_{0.15}PbI_3$ perovskite heterojunction under light illumination at zero bias. (e) UPS analysis of the $PtSe_2$ sample. Fermi level of the $PtSe_2$ film can be determined to be 4.84 eV. (f) Steady-state PL spectrum of the perovskite and $PtSe_2$/perovskite hybrid.

$$R = \frac{I_{ph}}{P_\lambda S} = \mathrm{EQE}\left(\frac{q\lambda}{hc}\right)G \quad (1)$$

where P_λ, S, q, λ, h, c, and G are the incident light intensity, the effective illuminated area (0.05 cm^2), the elementary charge, the light wavelength, Planck's constant, the speed of light, and photoconductive gain, respectively. G is unity in common photodiodes without an internal gain mechanism.[13,14] Therefore, according to the equation, R and EQE were estimated to be 117.7 mA W^{-1} and 14.9%, respectively, under low light intensity at zero bias. The R value is lower than that of a $PtSe_2$/Si (490 mAW^{-1}) heterojunction photodetector[27] but is slightly higher than that of a self-driven $CH_3NH_3PbI_xCl_{3-x}$ perovskite photodetector on carbon cloth at this wavelength region (~100 mA W^{-1}).[38] In addition, the EQE value is superior to that of a self-driven $CsPbBr_3$ single-crystal-based Schottky junction photodetector (~6%).[39] Figure 3f illustrates the R and EQE as a function of light intensity. Because of increased carrier recombination activity at higher light intensity, both values decreased with increasing light intensity.

Next, we studied the specific detectivity (D^*), which is another key parameter of a photodetector and is given by

$$D^* = \frac{(A\Delta f)^{1/2}}{\mathrm{NEP}} \quad (2)$$

$$\mathrm{NEP} = \frac{\overline{i_n^2}^{1/2}}{R} \quad (3)$$

where A, Δf, NEP, and $\overline{i_n^2}^{1/2}$ are the effective area of the device (0.06 cm^2), bandwidth, noise equivalent power, and root-mean-square value of the noise current, respectively. The $\overline{i_n^2}^{1/2}$ was acquired by directly recording the noise current of the heterojunction device at different frequencies via a lock-in preamplifier. Figure 4a illustrates the $\overline{i_n^2}^{1/2}$ as a function of frequency, from which the noise level per unit bandwidth (1 Hz) of the device was deduced to be ~14 pA $Hz^{-1/2}$. Accordingly, a low threshold limit of NEP is estimated to be 1.19×10^{-10} W, which thereby gives a D^* value of 2.91×10^{12} Jones for the device at 808 nm at zero bias. Significantly, this value is slightly smaller than that of $CH_3NH_3PbI_3$·PbS solid/graphene photodetector[22] but is larger than that of previously reported 2D TMD/perovskite hybrid phototransistors including $MoS_2/CH_3NH_3PbI_3$,[17,18] $WS_2/CH_3NH_3PbI_3$,[19] and $WSe_2/CH_3NH_3PbI_3$[20] (see Table 1), suggesting that our photo-

DOI: 10.1021/acs.jpclett.8b00266
J. Phys. Chem. Lett. 2018, 9, 1185−1194

Table 1. Comparison of the Device Parameters of the Present $PtSe_2$/Perovskite Heterojunction Photodetector with Other 2D TMD/Perovskite-Based Devices Reported Previously

device structure	τ_r/τ_f	stability	D^* (Jones)	I_{light}/I_{dark} ratio	reference
$PtSe_2/FA_{0.85}Cs_{0.15}PbI_3$	78/60 ns (0 V); 74/55 ns (−0.5 V); 71/56 ns (−1 V)	three weeks	2.91×10^{12}	5.7×10^3	this work
$MoS_2/CH_3NH_3PbI_3$	6.2 s (5 V)	200 h	8.76×10^9	–	17
$WS_2/CH_3NH_3PbI_3$	2.7/7.5 ms (5 V)	–	2×10^{12}	10^5	19
$WSe_2/CH_3NH_3PbI_3$	<10 ms (0.5 V)	–	–	–	20
$CH_3NH_3PbI_3$/PDPP3T	30/150 ms (1 V)	14 days	1.5×10^{10}	–	21
$CH_3NH_3PbI_3$·PbS solid/graphene	>0.05 s (0.1 V)	–	5×10^{12}	–	22

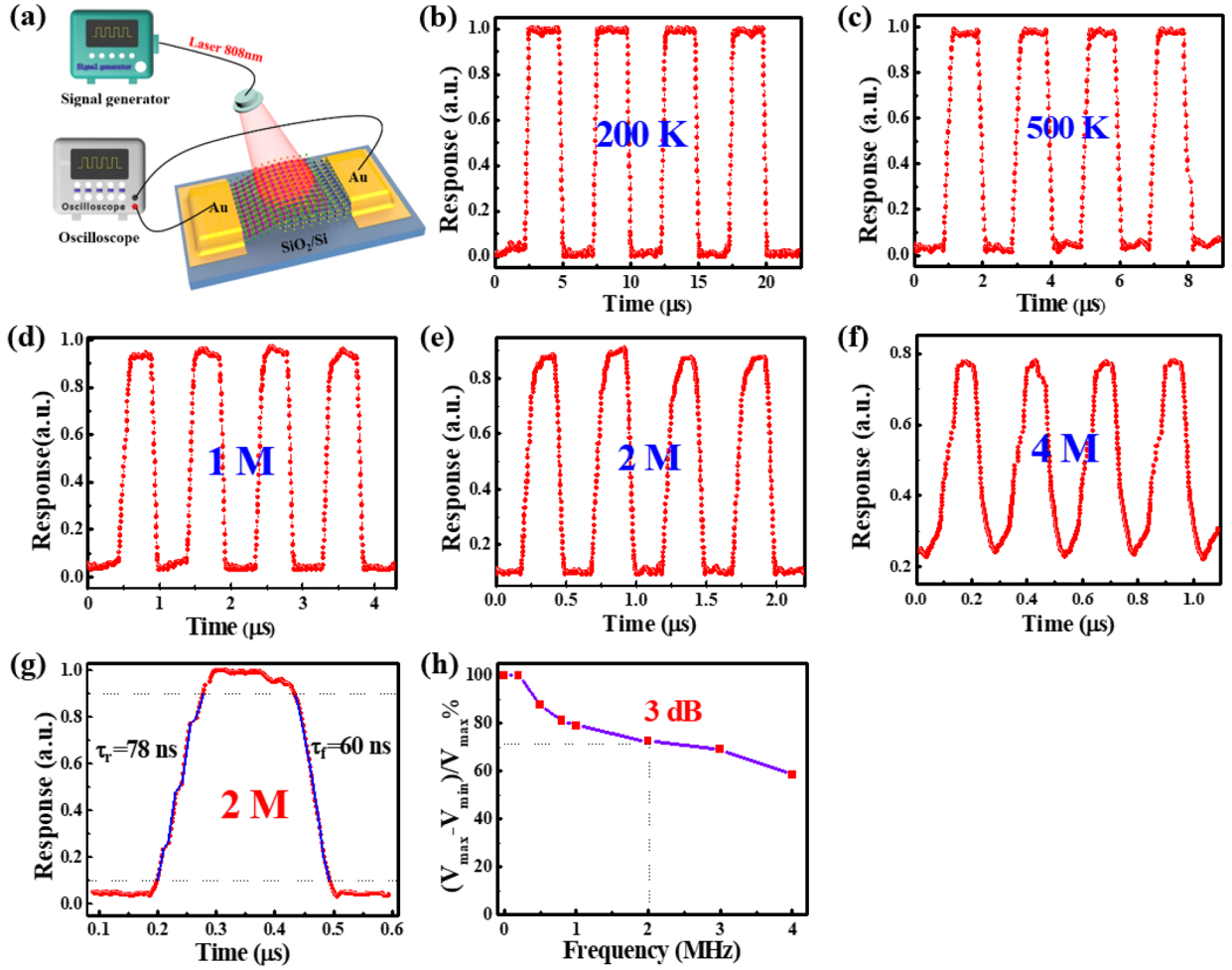

Figure 5. (a) Schematic illustration of the measurement setup for response speed measurement. Photoresponse of the device under pulsed NIR light illumination (808 nm) with the frequency of (b) 200 kHz, (c) 500 kHz, (d) 1 MHz, (e) 2 MHz, and (f) 4 MHz. (g) A single normalized cycle of the photoresponse for estimating rise and fall times. (h) Relative balance $(V_{max} - V_{min})/V_{max}$ versus switching frequency, showing the 3 dB cutoff frequency of ∼2 MHz.

detector can potentially detect weak light signal. Furthermore, the wavelength-dependent R and D^* of the $PtSe_2$/perovskite heterojunction photodetector were studied, as depicted in Figure 4b. It is evident that the device exhibited a broadband photoresponse from 300 to 1200 nm with peak response in the range from 700 to 900 nm. Even though the response is relatively low in the UV and NIR region, our heterojunction device is still capable of detecting both UV and NIR illuminations (Figure S5). Such a broadband photoresponse is directly related to the strong light absorption of the $PtSe_2$/perovskite hybrid in a wide wavelength region, as illustrated in Figure S4d. It is also interesting to note that the spectral response of our heterojunction device is in deep contrast to that of a pure $FA_{0.85}Cs_{0.15}PbI_3$ perovskite photodetector, which shows a sharp cutoff edge in spectral photoresponse at around 800 nm limited by the intrinsic optical absorption of perovskite.[30] The NIR photoresponse of the present device is associated with the excitation of electrons from the $PtSe_2$, which will be discussed later. In future study, it is expected that the NIR photoresponse can be further optimized by means of using perovskites with narrower band gap,[40] doping perovskites by introducing foreign atoms to form appropriate defect/trap centers within their band gap,[41] tuning the band gap of $PtSe_2$ via adjusting its thickness,[26] and integration with plasmonic nanostructures resonated at the NIR regime.[42]

The above photoresponse characteristics can be understood from the energy band diagram analysis illustrated in Figure 4c,d. The multilayer $PtSe_2$ film with a thickness of ∼15 nm can

DOI: 10.1021/acs.jpclett.8b00266
J. Phys. Chem. Lett. 2018, 9, 1185−1194

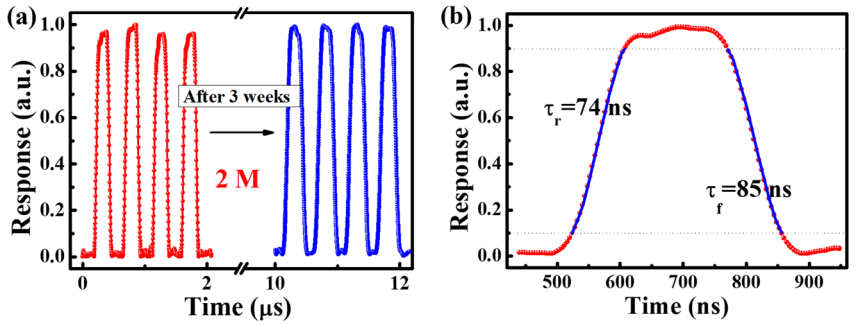

Figure 6. (a) Comparison of photoresponse of the device under pulsed NIR light (808 nm) with a frequency of 2 MHz before and after storage in ambient conditions for 3 weeks. (b) A single normalized cycle of the photoresponse after storage for estimating rise and fall times.

be deemed as a semimetal with zero band gap, and its Fermi level (E_F) was estimated to be 4.84 eV based on ultraviolet photoemission spectroscopy (UPS) measurement (Figure 4e). Moreover, $FA_{0.85}Cs_{0.15}PbI_3$ perovskite is a weak n-type semiconductor according to Hall effect testing results (data not shown here), and its conduction band minimum (E_C) and valence band maximum (E_V) values were obtained from a previous work.[43] Once the two materials are in contact with each other, because of the difference in Fermi levels, the electrons would diffuse from the perovskite to the $PtSe_2$ until the Fermi levels align, causing the energy levels near the perovskite surface to bend upward and eventually the formation of a built-in electric field near the $PtSe_2$/perovskite interface. As shown in Figure 4d, when the incident light with photon energy ($h\nu$) greater than the band gap of perovskite ($h\nu \geq E_g$, E_g = 1.52 eV, corresponding to absorption cutoff wavelength of about 815 nm),[32] excitons will be generated in the perovskite, and quickly dissociate into electrons and holes because of the low exciton binding energy.[44] When the incident light has photon energy greater than the heterojunction barrier height and less than the band gap of perovskite ($\Phi_B < h\nu < E_g$), electrons excited from the $PtSe_2$ can overcome the heterojunction barrier and are injected into the perovskite. The photogenerated electrons and holes near the heterojunction interface are rapidly separated by the built-in electric field, which ultimately form the photocurrent. The efficient separation of photogenerated electrons and holes is also evidenced by the significantly quenched photoluminesence (PL) intensity of $PtSe_2$/perovskite hybrid in comparison with the perovskite film (Figure 4f).[15]

Response speed is also a critical parameter of a photodetector, which signifies the capability of a photodetector to follow a rapidly varied optical signal. The response speed of the $PtSe_2$/perovskite heterojunction photodetector in this study was evaluated by a high-frequency optical signal that was provided by the NIR laser diode driven by a function generator (Figure 5a). Figure 5b–f displays the photoresponse of the heterojunction to pulsed light with different frequencies from 200 kHz to 4 MHz. All the photoresponses were normalized relative to an undamped photoresponse measured under 1 Hz pulsed light. Clearly, our photodetector exhibited excellent switching characteristics with a very fast photoresponse and good reproducibility under repeated on/off illumination for all measured frequencies of 200 kHz, 500 kHz, 1 MHz, 2 MHz, and 4 MHz. Notably, even under pulsed light with a frequency as high as 4 MHz, the photodetector can still follow the fast varied optical signal with distinct high and low photovoltage states. A single magnified photoresponse curve is illustrated in Figure 5g, from which the response speed was estimated to be 78 and 60 ns for rise and fall time at zero bias, respectively, according to the definition of response speed.[45] We also recorded the response speed under reverse bias of −0.5 V and −1 V, and the values are slightly faster than the response speed at zero bias, which is understandable because reverse bias can facilitate more efficient separation and transport of photocarriers. It is worth noting that the response speed of our device is much faster than that of other reported 2D TMDs/perovskite hybrid photodetectors (see Table 1) and is among the best results achieved for perovskite photodetectors to date.[3,4] Such an ultrafast photoresponse is related not only to the built-in electric field at the $PtSe_2$/perovskite interface but also to the unique electrical properties of both $PtSe_2$ and $FA_{0.85}Cs_{0.15}PbI_3$ perovskite. As discussed above, the built-in electric field is able to swiftly separate photogenerated carriers under illumination,[46] which is beneficial to response speed. On the other hand, the ultrafast response speed can also be attributed to the short transit time of photogenerated holes and electrons across the channel due to the relatively high charge carrier mobility of both materials. The field-effect hole mobility of the $PtSe_2$ film was estimated to be ∼4.31 $cm^2 s^{-1} V^{-1}$ (Figure S6), and the electron mobility of $FA_{0.85}Cs_{0.15}PbI_3$ perovskite was in the range of 54.6−157.1 $cm^2 s^{-1} V^{-1}$, which is measured using the Hall effect method. Such high carrier mobilities enable rapid drift of charge carriers under built-in or external applied potential, giving rise to short carrier transit times and thereby the fast photoresponse. In addition, the lower trap density as low as 1.75×10^{13} cm^{-3} for $FA_{0.85}Cs_{0.15}PbI_3$ in comparison with other perovskite materials can also contribute to the fast response speed by reducing the trapping probability of electrons.[30] In fact, we believe that the response speed can be further accelerated given the capacitance of the heterojunction or the thickness of the perovskite thin film are decreased. The photovoltage as a function of frequency was further studied (Figure 5h), which reveals a slow decay of the relative balance $(V_{max} - V_{min})/V_{max}$, and the relative balance decreases by only about 60% at a very high frequency of 4 MHz. In addition, the 3 dB frequency that is defined as the frequency at which the photoresponse drops from the maximum value to 0.707 of the maximum value was deduced to be ∼2 MHz. The combination of the above results implies that the $PtSe_2$/perovskite heterojunction photodetector can work well over a broad switching frequency range and is able to monitor ultrafast optical signals.

To evaluate the possibility of practical application, the air stability of the $PtSe_2$/perovskite heterojunction photodetector was then investigated by storing the sample in ambient conditions for 3 weeks without any encapsulation. Such good

DOI: 10.1021/acs.jpclett.8b00266
J. Phys. Chem. Lett. 2018, 9, 1185−1194

device stability can probably be ascribed to the relatively good material stability of both $PtSe_2$ and the perovskite thin film: First, unlike other TMD or black phosphorus materials,[47] the $PtSe_2$ used in this study is highly stable and can keep its structure as well as electrical property even after long-time storage in ambient conditions. Second, as revealed by a previously reported result, the $FAPbI_3$ thin film doped with Cs exhibited quite good stability. This is totally different from the previous study, in which the photodetectors made of methylammoniium lead halide (e.g., $CH_3NH_3PbX_3$, X = Cl, Br, I) perovskite materials often displayed unfavorable device instability when exposed at ambient conditions.[48] Figure 6a compares the photosensitivity before and after storage; it is found that the device can still display an excellent switching property, with the photoresponse remaining almost invariant, and good reproducibility under 2 MHz pulsed light after storage, suggesting good air stability and long-term durability of our heterojunction device. According to magnified individual cycle in Figure 6b, the rise and fall times after storage are determined to be 74 and 85 ns, respectively. Interestingly, we found that the rise time was almost unchanged while the fall time suffered somewhat from degradation. Such a slight variation in fall time can probably be related to the change of the structure of perovskite material after long-term storage at ambient conditions. As discovered in our previous work,[30] $CsPbI_3$ and some unknown phases will appear after storage likely because of the decomposition of $FA_{0.85}Cs_{0.15}PbI_3$ assisted by moisture in air at the surface of the perovskite.[49] The newly formed materials have optoelectronic characteristics different from those of $FA_{0.85}Cs_{0.15}PbI_3$ perovskite, which may cause variation in response speed.

In summary, an ultrafast, self-driven and air-stable heterojunction photodetector based on multilayer $PtSe_2$ and $FA_{0.85}Cs_{0.15}PbI_3$ perovskite has been successfully fabricated. Photoresponse analysis finds that such a heterojunction photodetector exhibited high sensitivity to illumination in a wide wavelength range from the UV to NIR spectrum region. The I_{light}/I_{dark} ratio, responsivity, and specific detectivity were estimated to be 5.7×10^3, 117.7 mA W^{-1} and 2.91×10^{12} Jones at zero bias, respectively, which are comparable to or better than those of other reported 2D TMDs/perovskite hybrid photodetectors. In addition, the device achieved ultrafast response speed with rise/fall times of 78/60 ns, making it among the fastest perovskite-2D photodetectors resported to date. These results signify that the present multilayer $PtSe_2$/perovskite heterojunction photodetector may find potential application for future air-stable, high-frequency optoelectronic devices.

EXPERIMENTAL SECTION

Material Synthesis and Characterization. The $PtSe_2$ film was synthesized by a facile selenization method. Briefly, ~5 nm Pt film was first deposited on a SiO_2/Si substrate via magnetron sputtering. Then, the Pt-coated substrate was placed at the center zone of a furnace, and selenium (Se) powder (99.99% in purity) was loaded at the upstream side. The powder was heated to its melting point (~220 °C) to allow evaporation, and Ar (50 sccm) was used as carrier gas. The temperature of the center zone of the furnace was set to be 380 °C. After selenization for 1 h, a thin film with gray appearance was obtained on the substrate. Figure S1 presents the schematic diagram of the synthesis processes of $PtSe_2$ film.

The $FA_{0.85}Cs_{0.15}PbI_3$ perovskite film was prepared according to a previously reported method.[30] The precursor solution was first obtained by dissolving 461 mg of PbI_2 (Aldrich, 99%), 38.9 mg of CsI (Aldrich, 99.9%), and 145 mg of FAI (Aldrich, 99.5%) sequentially into a mixed solvent of 200 μL of dimethyl sulfoxide (DMSO, > 99.9%) and 800 μL of *N*,*N*-dimethylformamide (DMF, 99.8%) and stirred at 70 °C for 1 h before use. Then, 40 μL of the precursor solution was spin-coated onto a glass substrate at 4000 rpm. After 10 s, 100 μL of diethyl ether (99.0%) was dripped slowly onto the rotating substrate. After spin-coating for another 50 s, the substrate was sequentially annealed at 50 °C for 3 min and then 140 °C for 15 min. Eventually, the perovskite film in black-brownish color was obtained.

The morphology of $PtSe_2$ and perovskite was observed using a FESEM instrument (Hitachi, SU8020). The XPS measurement of $PtSe_2$ was performed using a monochromatic Al Kα source (1486.6 eV) produced by the XPS system. The topography of $PtSe_2$ was obtained by atomic force microscopy (AFM, Benyuan Nanotech Com, CSPM-4000). The crystal structure of $PtSe_2$ was probed using a FETEM instrument (JEOL model JEM-2100F). The Raman spectrum and mapping of $PtSe_2$ were recorded on a HR Evolution (Horiba Jobin Yvon) Raman spectrometer with a 532 nm laser. The absorption spectra of $PtSe_2$, perovskite, and $PtSe_2$/perovskite hybrid films on glass substrates were recorded on a Shimadzu UV-2550 UV−vis spectrophotometer. The XRD pattern of perovskite was recorded using an X-ray diffractormeter (Rigaku D/max-rB). The PL spectra was explored by a confocal laser Raman spectrometer (Horiba Jobin Yvon, Labram HR evolution).

Device Fabrication and Analysis. To fabricate the $PtSe_2$/perovskite heterojunction device, the perovskite precursor solution was spin-coated onto a SiO_2/Si substrate partially covered with $PtSe_2$ film, and the volume of the solution was carefully controlled to avoid full coverage of perovskite on the substrate. The heterojunction was formed at the region where $PtSe_2$ and perovskite are overlapped. Parallel Au electrodes with a thickness of ~50 nm was deposited via an electron-beam evaporator using a homemade shadow mask to form separate Ohmic contacts to $PtSe_2$ and perovskite. Figure S2 schematically shows the fabrication procedures of the $PtSe_2$/perovskite heterojunction device. The electrical measurements of the heterojunction device were conducted using a semiconductor characterization system (4200-SCS, Keithley Co. Ltd.). An 808 nm laser diode (Tanon Company, UV-100) was used to illuminate the device for optoelectronic property investigation. For response speed study, a signal generator (Tektronix, TDS2022B) was employed to drive the laser diode to produce a high-frequency incident light, and an oscilloscope (Tektronix, TDS2012B) was used to record the electrical data. The power intensity of all light sources was carefully calibrated using a power meter (Thorlabs GmbH., PM 100D) before measurement. All measurements were performed in air at room temperature.

ASSOCIATED CONTENT

Supporting Information

The Supporting Information is available free of charge on the ACS Publications website at DOI: 10.1021/acs.jpclett.8b00266.

Synthetic setup for preparing the $PtSe_2$ thin film, device fabrication process, XPS analysis of the $PtSe_2$, structural

DOI: 10.1021/acs.jpclett.8b00266
J. Phys. Chem. Lett. 2018, 9, 1185−1194

and optical analyses of both $PtSe_2$ and perovskite thin film, photoresponse of the device, and calculation of hole mobility of the $PtSe_2$ film (PDF)

AUTHOR INFORMATION

Corresponding Authors

*E-mail: chao.xie@hfut.edu.cn.
*E-mail: luolb@hfut.edu.cn.
*E-mail: ycwu@hfut.edu.cn.

ORCID

Chao Xie: 0000-0003-4451-767X
Yuen Hong Tsang: 0000-0001-5632-5224
Lin-Bao Luo: 0000-0001-8651-8764

Author Contributions

‖Z.-X.Z. and L.-H.Z. contributed equally.

Notes

The authors declare no competing financial interest.

ACKNOWLEDGMENTS

This work was supported by the National Natural Science Foundation of China (NSFC; Nos. 61675062, 61575059, and 21501038), the Fundamental Research Funds for the Central Universities (2013HGCH0012 and 2014HGCH0005), and the China Postdoctoral Science Foundation (103471013).

REFERENCES

(1) Zhao, Y.; Zhu, K. Organic−inorganic Hybrid Lead Halide Perovskites for Optoelectronic and Electronic Applications. *Chem. Soc. Rev.* **2016**, *45*, 655−689.
(2) Chen, Q.; De Marco, N.; Yang, Y.; Song, T.-B.; Chen, C. C.; Zhao, H.; Hong, Z.; Zhou, H.; Yang, Y. Under the Spotlight: The Organic-Inorganic Hybrid Halide Perovskite for Optoelectronic Applications. *Nano Today* **2015**, *10*, 355−396.
(3) Wang, H.; Kim, D. H. Perovskite-Based Photodetectors: Materials and Devices. *Chem. Soc. Rev.* **2017**, *46*, 5204−5236.
(4) Ahmadi, M.; Wu, T.; Hu, B. A Review on Organic-Inorganic Halide Perovskite Photodetectors: Device Engineering and Fundamental Physics. *Adv. Mater.* **2017**, *29*, 1605242.
(5) Tian, W.; Zhou, H.; Li, L. Hybrid Organic-Inorganic Perovskite Photodetectors. *Small* **2017**, *13*, 1702107.
(6) Zhou, J.; Huang, J. Photodetectors Based on Organic-Inorganic Hybrid Lead Halide Perovskites. *Adv. Sci.* **2018**, *5*, 1700256.
(7) Dou, L.; Yang, Y.; You, J.; Hong, Z.; Chang, W.-H.; Li, G.; Yang, Y. Solution-Processed Hybrid Perovskite Photodetectors with High Detectivity. *Nat. Commun.* **2014**, *5*, 5404.
(8) Fang, Y.; Huang, J. Resolving Weak Light of Sub-Picowatt per Square Centimeter by Hybrid Perovskite Photodetectors Enabled by Noise Reduction. *Adv. Mater.* **2015**, *27*, 2804−2810.
(9) Lin, Q.; Armin, A.; Lyons, D. M.; Burn, P. L.; Meredith, P. Low Noise, IR-Blind Organohalide Perovskite Photodiodes for Visible Light Detection and Imaging. *Adv. Mater.* **2015**, *27*, 2060−2064.
(10) Shen, L.; Fang, Y.; Wang, D.; Bai, Y.; Deng, Y.; Wang, M.; Lu, Y.; Huang, J. A Self-Powered, Sub-Nanosecond-Response Solution-Processed Hybrid Perovskite Photodetector for Time-Resolved Photoluminescence-Lifetime Detection. *Adv. Mater.* **2016**, *28*, 10794−10800.
(11) Koppens, F. H. L.; Mueller, T.; Avouris, P.; Ferrari, A. C.; Vitiello, M. S.; Polini, M. Photodetectors Based on Graphene, Other Two-Dimensional Materials and Hybrid Systems. *Nat. Nanotechnol.* **2014**, *9*, 780−793.
(12) Li, J.; Niu, L.; Zheng, Z.; Yan, F. Photosensitive Graphene Transistors. *Adv. Mater.* **2014**, *26*, 5239−5273.
(13) Buscema, M.; Island, J. O.; Groenendijk, D. J.; Blanter, S. I.; Steele, G. A.; van der Zant, H. S. J.; Castellanos-Gomez, A. Photocurrent Generation with Two-Dimensional van Der Waals Semiconductors. *Chem. Soc. Rev.* **2015**, *44*, 3691−3718.
(14) Xie, C.; Mak, C.; Tao, X.; Yan, F. Photodetectors Based on Two-Dimensional Layered Materials Beyond Graphene. *Adv. Funct. Mater.* **2017**, *27*, 1603886.
(15) Lee, Y.; Kwon, J.; Hwang, E.; Ra, C. H.; Yoo, W. J.; Ahn, J. H.; Park, J. H.; Cho, J. H. High-Performance Perovskite-Graphene Hybrid Photodetector. *Adv. Mater.* **2015**, *27*, 41−46.
(16) Wang, Y.; Zhang, Y.; Lu, Y.; Xu, W.; Mu, H.; Chen, C.; Qiao, H.; Song, J.; Li, S.; Sun, B.; et al. Hybrid Graphene-Perovskite Phototransistors with Ultrahigh Responsivity and Gain. *Adv. Opt. Mater.* **2015**, *3*, 1389−1396.
(17) Kang, D.; Pae, S. R.; Shim, J.; Yoo, G.; Jeon, J.; Leem, J. W.; Yu, J. S.; Lee, S.; Shin, B.; Park, J. An Ultrahigh-Performance Photodetector Based on a Perovskite-Transition-Metal-Dichalcogenide Hybrid Structure. *Adv. Mater.* **2016**, *28*, 7799−7806.
(18) Wang, Y.; Fullon, R.; Acerce, M.; Petoukhoff, C. E.; Yang, J.; Chen, C.; Du, S.; Lai, S. K.; Lau, S. P.; Voiry, D.; et al. Solution-Processed MoS_2/Organolead Trihalide Perovskite Photodetectors. *Adv. Mater.* **2017**, *29*, 1603995.
(19) Ma, C.; Shi, Y.; Hu, W.; Chiu, M.-H.; Liu, Z.; Bera, A.; Li, F.; Wang, H.; Li, L.-J.; Wu, T. Heterostructured $WS_2/CH_3NH_3PbI_3$ Photoconductors with Suppressed Dark Current and Enhanced Photodetectivity. *Adv. Mater.* **2016**, *28*, 3683−3689.
(20) Lu, J.; Carvalho, A.; Liu, H.; Lim, S. X.; Castro Neto, A. H.; Sow, C. H. Hybrid Bilayer $WSe_2-CH_3NH_3PbI_3$ Organolead Halide Perovskite as a High-Performance Photodetector. *Angew. Chem., Int. Ed.* **2016**, *55*, 11945−11949.
(21) Chen, S.; Teng, C.; Zhang, M.; Li, Y.; Xie, D.; Shi, G. A Flexible UV-Vis-NIR Photodetector Based on a Perovskite/Conjugated-Polymer Composite. *Adv. Mater.* **2016**, *28*, 5969−5974.
(22) Bessonov, A. A.; Allen, M.; Liu, Y.; Malik, S.; Bottomley, J.; Rushton, A.; Medina-Salazar, I.; Voutilainen, M.; Kallioinen, S.; Colli, A.; et al. Compound Quantum Dot-Perovskite Optical Absorbers on Graphene Enhancing Short-Wave Infrared Photodetection. *ACS Nano* **2017**, *11*, 5547−5557.
(23) Xie, C.; You, P.; Liu, Z.; Li, L.; Yan, F. Ultrasensitive Broadband Phototransistors Based on Perovskite/organic-Semiconductor Vertical Heterojunctions. *Light: Sci. Appl.* **2017**, *6*, e17023.
(24) Xie, C.; Yan, F. Perovskite/Poly(3-hexylthiophene)/Graphene Multiheterojunction Phototransistors with Ultrahigh Gain in Broadband Wavelength Region. *ACS Appl. Mater. Interfaces* **2017**, *9*, 1569−1576.
(25) Cheng, H.-C.; Wang, G.; Li, D.; He, Q.; Yin, A.; Liu, Y.; Wu, H.; Ding, M.; Huang, Y.; Duan, X. Van Der Waals Heterojunction Devices Based on Organohalide Perovskites and Two-Dimensional Materials. *Nano Lett.* **2016**, *16*, 367−373.
(26) Zhao, Y.; Qiao, J.; Yu, Z.; Yu, P.; Xu, K.; Lau, S. P.; Zhou, W.; Liu, Z.; Wang, X.; Ji, W.; et al. High-Electron-Mobility and Air-Stable 2D Layered $PtSe_2$ FETs. *Adv. Mater.* **2017**, *29*, 1604230.
(27) Yim, C.; Lee, K.; McEvoy, N.; O'Brien, M.; Riazimehr, S.; Berner, N. C.; Cullen, C. P.; Kotakoski, J.; Meyer, J. C.; Lemme, M. C.; et al. High-Performance Hybrid Electronic Devices from Layered $PtSe_2$ Films Grown at Low Temperature. *ACS Nano* **2016**, *10*, 9550−9558.
(28) Wang, Z.; Li, Q.; Besenbacher, F.; Dong, M. Facile Synthesis of Single Crystal $PtSe_2$ Nanosheets for Nanoscale Electronics. *Adv. Mater.* **2016**, *28*, 10224−10229.
(29) Wang, Y.; Li, L.; Yao, W.; Song, S.; Sun, J. T.; Pan, J.; Ren, X.; Li, C.; Okunishi, E.; Wang, Y. Q.; et al. Monolayer $PtSe_2$, a New Semiconducting Transition-Metal Dichalcogenide, Epitaxially Grown by Direct Selenization of Pt. *Nano Lett.* **2015**, *15*, 4013−4018.
(30) Liang, F.-X.; Wang, J.-Z.; Zhang, Z.-X.; Wang, Y.-Y.; Gao, Y.; Luo, L.-B. Broadband, Ultrafast, Self-Driven Photodetector Based on Cs-Doped $FAPbI_3$ Perovskite Thin Film. *Adv. Opt. Mater.* **2017**, *5*, 1700654.
(31) Ndione, P. F.; Li, Z.; Zhu, K. Effects of Alloying on the Optical Properties of Organic−inorganic Lead Halide Perovskite Thin Films. *J. Mater. Chem. C* **2016**, *4*, 7775−7782.

DOI: 10.1021/acs.jpclett.8b00266
J. Phys. Chem. Lett. 2018, 9, 1185−1194

(32) Li, Z.; Yang, M.; Park, J. S.; Wei, S. H.; Berry, J. J.; Zhu, K. Stabilizing Perovskite Structures by Tuning Tolerance Factor: Formation of Formamidinium and Cesium Lead Iodide Solid-State Alloys. *Chem. Mater.* **2016**, *28*, 284−292.
(33) Ullah, K.; Ye, S.; Lei, Z.; Cho, K. Y.; Oh, W. C. Synergistic Effect of $PtSe_2$ and Graphene Sheets Supported by TiO_2 as Cocatalysts Synthesized via Microwave Techniques for Improved Photocatalytic Activity. *Catal. Sci. Technol.* **2015**, *5*, 184−198.
(34) O'Brien, M.; McEvoy, N.; Motta, C.; Zheng, J.-Y.; Berner, N. C.; Kotakoski, J.; Elibol, K.; Pennycook, T. J.; Meyer, J. C.; Yim, C.; et al. Raman Characterization of Platinum Diselenide Thin Films. *2D Mater.* **2016**, *3*, 021004.
(35) Wang, L.; Jie, J.; Shao, Z.; Zhang, Q.; Zhang, X.; Wang, Y.; Sun, Z.; Lee, S.-T. MoS_2/Si Heterojunction with Vertically Standing Layered Structure for Ultrafast, High-Detectivity, Self-Driven Visible-Near Infrared Photodetectors. *Adv. Funct. Mater.* **2015**, *25*, 2910−2919.
(36) Li, X.; Zhu, M.; Du, M.; Lv, Z.; Zhang, L.; Li, Y.; Yang, Y.; Yang, T.; Li, X.; Wang, K.; et al. High Detectivity Graphene-Silicon Heterojunction Photodetector. *Small* **2016**, *12*, 595−601.
(37) Xie, C.; Yan, F. Flexible Photodetectors Based on Novel Functional Materials. *Small* **2017**, *13*, 1701822.
(38) Sun, H.; Lei, T.; Tian, W.; Cao, F.; Xiong, J.; Li, L. Self-Powered, Flexible, and Solution-Processable Perovskite Photodetector Based on Low-Cost Carbon Cloth. *Small* **2017**, *13*, 1701042.
(39) Saidaminov, M. I.; Haque, M. A.; Almutlaq, J.; Sarmah, S.; Miao, X. H.; Begum, R.; Zhumekenov, A. A.; Dursun, I.; Cho, N.; Murali, B.; et al. Inorganic Lead Halide Perovskite Single Crystals: Phase-Selective Low-Temperature Growth, Carrier Transport Properties, and Self-Powered Photodetection. *Adv. Opt. Mater.* **2017**, *5*, 1600704.
(40) Hao, F.; Stoumpos, C. C.; Guo, P.; Zhou, N.; Marks, T. J.; Chang, R. P. H.; Kanatzidis, M. G. Solvent-Mediated Crystallization of $CH_3NH_3SnI_3$ Films for Heterojunction Depleted Perovskite Solar Cells. *J. Am. Chem. Soc.* **2015**, *137*, 11445−11452.
(41) Zhou, Y.; Yong, Z. J.; Zhang, K. C.; Liu, B. M.; Wang, Z. W.; Hou, J. S.; Fang, Y. Z.; Zhou, Y.; Sun, H. T.; Song, B. Ultrabroad Photoluminescence and Electroluminescence at New Wavelengths from Doped Organometal Halide Perovskites. *J. Phys. Chem. Lett.* **2016**, *7*, 2735−2741.
(42) Wang, W.; Klots, A.; Prasai, D.; Yang, Y.; Bolotin, K. I.; Valentine, J. Hot Electron-Based Near-Infrared Photodetection Using Bilayer MoS_2. *Nano Lett.* **2015**, *15*, 7440−7444.
(43) Xia, X.; Wu, W.; Li, H.; Zheng, B.; Xue, Y.; Xu, J.; Zhang, D.; Gao, C.; Liu, X. Spray Reaction Prepared FA $_{1-X}Cs_XPbI_3$ Solid Solution as a Light Harvester for Perovskite Solar Cells with Improved Humidity Stability. *RSC Adv.* **2016**, *6*, 14792−14798.
(44) Fang, H.; Wang, F.; Adjokatse, S.; Zhao, N.; Even, J.; Loi, M. A. Photoexcitation Dynamics in Solution- Processed Formamidinium Lead Iodide Perovskite Thin Films for Solar Cell Applications Running Title:Optical Properties of a Hybrid Perovskite. *Light: Sci. Appl.* **2016**, *5*, e16056.
(45) Zeng, L. H.; Wang, M. Z.; Hu, H.; Nie, B.; Yu, Y. Q.; Wu, C. Y.; Wang, L.; Hu, J. G.; Xie, C.; Liang, F. X.; et al. Monolayer Graphene/Germanium Schottky Junction as High-Performance Self-Driven Infrared Light Photodetector. *ACS Appl. Mater. Interfaces* **2013**, *5*, 9362−9366.
(46) Xie, C.; Nie, B.; Zeng, L.; Liang, F.-X.; Wang, M.-Z.; Luo, L.; Feng, M.; Yu, Y.; Wu, C.-Y.; Wu, Y.; et al. Core−Shell Heterojunction of Silicon Nanowire Arrays and Carbon Quantum Dots for Photovoltaic Devices and Self-Driven Photodetectors. *ACS Nano* **2014**, *8*, 4015−4022.
(47) Chen, C.; Youngblood, N.; Peng, R. M.; Yoo, D.; Mohr, D. A.; Johnson, T. W.; Oh, S. H.; Li, M. Three-Dimensional Integration of Black Phosphorus Photodetector with Silicon Photonics and Nano-plasmonics. *Nano Lett.* **2017**, *17*, 985−991.
(48) Guo, Y. L.; Liu, C.; Tanaka, H.; Nakamura, E. Air-Stable and Solution-Processable Perovskite Photodetectors for Solar-Blind UV and Visible Light. *J. Phys. Chem. Lett.* **2015**, *6*, 535−539.
(49) Brinkmann, K. O.; Zhao, J.; Pourdavoud, N.; Becker, T.; Hu, T.; Olthof, S.; Meerholz, K.; Hoffmann, L.; Gahlmann, T.; Heiderhoff, R.; et al. Suppressed Decomposition of Organometal Halide Perovskites by Impermeable Electron-Extraction Layers in Inverted Solar Cells. *Nat. Commun.* **2017**, *8*, 13938.

DOI: 10.1021/acs.jpclett.8b00266
J. Phys. Chem. Lett. 2018, 9, 1185−1194